Enhanced Electrical Conductivity of Silver Nanoparticles for High Frequency Electronic Applications

Ali H. Alshehri,[†] Malgorzata Jakubowska,[‡,§] Anna Młożniak,[§] Michal Horaczek,[‡] Diana Rudka,[‡] Charles Free,[†] and J. David Carey*,[†]

[†]Advanced Technology Institute, University of Surrey, Guildford, GU2 7XH, United Kingdom
[‡]Faculty of Mechatronics, Warsaw University of Technology, Warsaw, Poland
[§]Institute of Electronic Materials Technology, Warsaw, Poland

ABSTRACT: An enhancement in the electrical performance of low temperature screen-printed silver nanoparticles (nAg) has been measured at frequencies up to 220 GHz. We show that for frequencies above 80 GHz the electrical losses in coplanar waveguide structures fabricated using nAg at 350 °C are lower than those found in conventional thick film Ag conductors consisting of micrometer-sized grains and fabricated at 850 °C. The improved electrical performance is attributed to the better packing of the silver nanoparticles resulting in lower surface roughness by a factor of 3. We discuss how the use of silver nanoparticles offers new routes to high frequency applications on temperature sensitive conformal substrates and in sub-THz metamaterials.

KEYWORDS: silver nanoparticles, high frequency conduction, GHz and sub-THz characteristics, surface roughness, antenna materials, metamaterials
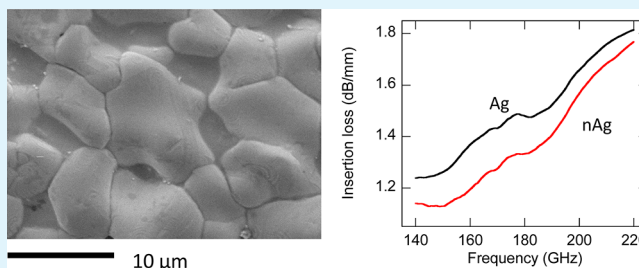
1. INTRODUCTION

Materials composed of metallic nanoparticles often exhibit strikingly different properties when compared with their bulk counterparts. The higher proportion of atoms on the surface of nanoparticles tends to result in higher surface free energies and greater chemical reactivity. This enhanced reactivity of metallic nanoparticles has attracted considerable attention as potential catalyst materials,[1] for improved gas sensor performance[2] and at THz and optical frequencies associated plasmonic[3] effects lead to enhanced light adsorption in solar cells.[4] Metallic nanoparticles can be used in surface enhanced Raman spectroscopy[5] for molecular and bimolecular identification. A key material property of metallic nanomaterials is their lower melting temperature compared with bulk metals.[6] For example, the melting point of bulk silver is 960 °C, whereas silver nanoparticles have a lower melting temperature which depends upon their diameter via the Gibbs−Thomson effect.[7,8] For example, Yeschenko et al.[9] showed that the melting point of silver nanoparticles embedded in a silica matrix varied between 350 °C (30 nm diameter) and 160 °C (8 nm diameter). A reduction in the melting temperature was also seen recently by Little et al. for silver films formed into nanometer sized islands on Si substrates;[10] both approaches employed optical (plasmon based) methods to determine the onset of melting. Although the Gibbs−Thompson description is widely employed, Gunawan and Johari showed that in more complicated systems, such as 30 nm diameter Zn (core) nanoparticles with a ZnO (shell) coating, the reduction in melting temperature from the bulk value was considerably less (only by 1−2 °C).[11] They attributed this to a complex interaction between the Zn core and oxide shell and concluded that the Gibbs−Thompson description is valid when the melting species is in equilibrium with its vapor and when it is not confined. This is an important consideration for nanometallic composite material systems which possess a low metallic content. As a consequence to make full use of the lower melting temperature, most studies, including this one, have high metallic content and this gives rise to an important processing advantage over bulk metals in which lower temperatures (200−400 °C) can be used using conventional thermal, laser annealing[12,13] or electrical heating.[14] The resultant materials can find use in a wide range of applications including as the conductive layer in printable electronics and the development of inkjet printable metal components.[14] An advantage of using lower temperatures up to 400 °C is that it facilitates the use of temperature sensitive substrates; for example the use of the polyimide film Kapton for flexible circuits and large area electronics. In the area of rf and microwave engineering applications include printable cylindrical antennas arrays for all-round radar coverage,[15,16] and for ultrawide band antennas on paper,[17] as well as conformal and flexible surfaces that need to be tolerant to mechanical bending are required.

The very high frequency electrical characterization of such metallic nanoparticle based conductors is in its infancy where the millimeter frequency (sub-THz) band response is largely unexplored. Split-ring resonator (SRR) structures using silver nanoparticles have been fabricated into arrays on flexible polyimide substrates and have demonstrated metamaterial behavior (resonances in transmission) up to 500 GHz.[18] As a consequence a key issue in metallic nanoparticle-based metamaterials, and electrical conductors in general, is to understand the factors that influence the high frequency losses. The principal objective of this study is therefore to study the high frequency (up to 220 GHz) electrical characteristics of screen printed metallic conductors composed of silver nanoparticles sintered at 350 °C. Structural and electrical comparison will be made with silver samples with micrometer-sized grains produced at 850 °C. We show that the electrical losses of lower temperature sintered silver nanoparticle conductors are lower than that of micrometer-sized silver. It will be further shown that this is due to the lower surface roughness resulting from improved atomic packing which in turn arises from the lower melting point of nanometallic silver. We also compare the high frequency electrical behavior of the metallic conductors with that of carbon nanotube-polymer composites as representative examples of nanomaterials with different relative contents of conductive to nonconductive phase. In doing so, we can draw conclusions about the factors that control the high frequency conduction in nanomaterial systems.

2. EXPERIMENTAL SECTION

2.1. Sample Preparation. Two types of silver material are examined in this study: one consisting of nanometallic silver and one consisting of micrometer-sized grains. Both types are produced by a thick film fabrication process. The thick film fabrication process consists of materials usually composed of (i) fine metal powder, (ii) an inorganic binder, such as a metal oxide, and (iii) an organic vehicle that evaporates during the initial drying process. After firing the metal particles atoms stick to each other and form strong bonding and dense atomic packing. In this study, "conventional thick film silver" refers to the use of micrometer sized silver grains; nAg refers to nanoparticles of Ag with the inorganic binder replaced by polymethyl methacrylate (PMMA). Nanoparticles of silver (up to 18 nm diameter before heating) were obtained from the thermal decomposition of silver salts of palmitic acid followed by pregrounding and ultrasonic agitation. The powders were then placed in a container and mixed with PMMA as a binder and a solution of butyl carbitol acetate. The nanomaterial samples consist of 82 wt % silver nanoparticles powder with 8 wt % PMMA in 10 wt % butyl carbitol acetate. The thick film silver samples have 81.5% Ag mixed with an oxide bond and were fired at 850 °C for 6 h.

2.2. Screen Printing and Coplanar Waveguide Fabrication. High frequency electrical characterization can be performed by fabricating the samples into a three electrode configuration known as a coplanar waveguide (CPW) in which the electrical signal is sent down a central line with two ground lines either side (Figure 1a). This is known as the ground-signal-ground electrode geometry. Prior to screen printing of the samples under investigation, pure silver photoimageable contact pads were first printed, exposed to UV light for one second using an MA3 (Hibridas) exposure unit and then developed using 0.2% aqueous solution of ethanolamine, fired at 850 °C and are 50 Ω matched. After the contact pads were produced the Ag or nAg pastes were screen printed (with the pastes attached to the contact pads) and fired them at 850 and 350 °C, respectively. Both types of sample were screen printed unto 96% purity alumina substrate (Coors Tek Ltd., type: AD-96) of 635 μm thickness to form CPW structures (Figure 1a). The lengths of the CPWs were between 5 mm
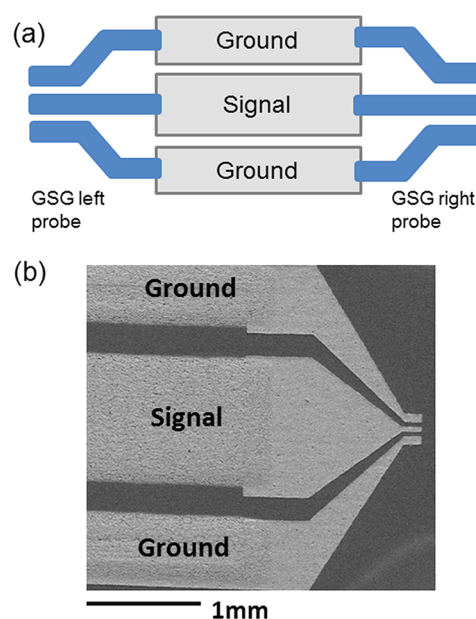

Figure 1. (a) Schematic electrode setup showing the ground–signal–ground (GSG) geometry. (b) Scanning electron microscope image showing part of the CPW and the contact pad in the GSG geometry. The total length of the conductors ranges from 5 to 25 mm; only part of the CPW with the contact pads (on the right-hand side) is shown.

and 25 mm and were attached to photoimageable pure silver contact pad. After printing of the electrode pads, the nAg CPWs were then dried to remove volatile solvents and then sintered at 350 °C for 1.5 h which removed the majority of the organic residue. The coplanar lines exhibited good adhesion to the alumina substrates and the coplanar lines track widths were designed to be 400 (for the outer ground tracks), 1400 (for the central signal track), and 320 μm (for the gap between the outer and central signal tracks) (Figure 1b). The cross-section of the tracks is rectangular with a thickness of the tracks (postfiring) of approximately 20 μm (based on Alfa Step micrometer measurements). The shape and thickness of the CPW of both Ag and nAg samples are the same and are determined by the screen specifications.

2.3. Surface Structural Characterization. Surface structural analysis was performed using a FEI Quanta 200 scanning electron microscope and a Veeco Digital Instruments Dimension 3100 atomic force microscope (AFM). From Figure 2a and b, it can be seen that the surface of the thick film silver sample is considerably rougher than that found in the sample made from nanoparticle silver, Figure 2c and d. Analysis of the root-mean-square (rms) roughness obtained from the AFM images indicated that the thick film silver sample has an average rms roughness of 465 nm (standard deviation of 38 nm obtained from nine measurements) compared to that of 151 nm (standard deviation of 25 nm from nine measurements) for the nAg samples. As a consequence the average rms roughness of samples made with nanosilver is approximately 1/3 that of samples made of micrometer-sized Ag and is attributed to the silver nanoparticles being close packed (Figure 2c and d).

2.4. Electrical Characterization. Electrical characterization of the CPWs has been performed in the frequency range of 45 MHz to 110 GHz and from 140 to 220 GHz. The electrical characteristics (scattering S-parameters) of the samples were measured using a HP 8510C vector network analyzer.[19] Here the S_{21} insertion loss, L, is presented in both dB per unit length (dB/mm) and dB per wavelength (dB/λ); the latter quantity being a key design parameter since many dimensions in high frequency electronics are specified as a fraction of a wavelength, for example, a half-wavelength filter or a quarter-wavelength coupler. The insertion loss per wavelength was found by converting the physical length, l, of the conductor to its corresponding electrical length.[20] A low-loss gold standard electrode (length 0.2 mm)
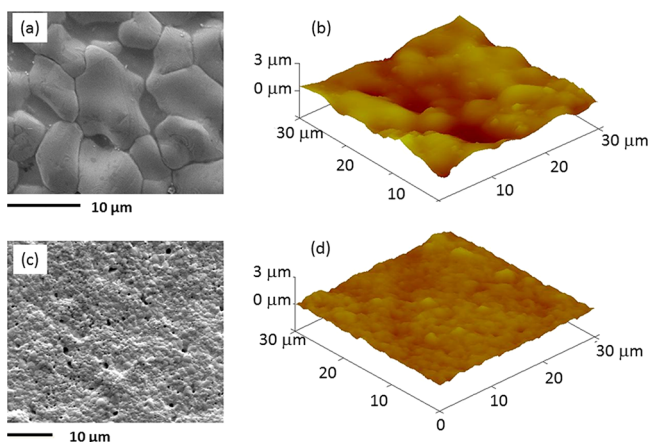
Figure 2. Surface of thick film silver sample viewed under (a) scanning electron microscope and (b) AFM. The surface of nanosilver *n*Ag sample viewed under (c) scanning electron microscope and (d) AFM. Analysis of the AFM data taken from nine locations on both samples shows that the thick film silver sample is approximately three times rougher than that of the nanosilver samples.

was used as a reference sample and losses per unit length as a function of frequency were found from eq 1

$$\text{loss(dB/mm)} = \frac{L - L_{\text{ref}}}{l - l_{\text{ref}}} \tag{1}$$

Defining the signal loss in this way has the advantage of removing any system errors in the measurement and allows us to avoid the need to remove the impedance mismatch at the probe–circuit interface using a de-embedding procedure. The average signal loss calculated from measurements made on five different Ag and five different *n*Ag samples is presented in Figure 3.

3. RESULTS AND DISCUSSION

In the lower frequency range, Figure 3a, the average behavior of both types of conductors is similar with the electrical loss increasing approximately linearly with frequency at a rate of approximately 0.1 dB/mm per GHz up to about 80 GHz. Above 80 GHz the electrical losses from the samples fabricated with *n*Ag are found to be lower and this behavior is continued throughout the whole of the higher frequency range, Figure 3b, from 140 to 220 GHz. In Figure 3c, the loss characteristics shown in Figure 3b are plotted in terms of loss per unit wavelength (dB/λ). The measured average loss from the *n*Ag samples is 0.067 dB/λ (standard deviation of 0.002 dB/λ), less than the losses found in the thick film Ag which was 0.073 dB/λ (standard deviation of 0.002 dB/λ). To put these loss figures in context, in a previous study of carbon nanotube–polymer composites conductors[19] the loss per wavelength in the same frequency range was a factor of 3 times larger at about 0.2 dB/λ. It is also interesting to note the lower level of the loss from the *n*Ag CPWs and that the overall trend in loss per wavelength does not depend significantly on frequency. This conclusion is significant and indicates that the electrical loss at these frequencies will become independent of the electrical size of a passive component or in a metamaterial structure.

With these results in mind it is therefore immediately tempting to try to extract the capacitance, inductances and resistances per unit length using the standard textbook analysis[20] to quantify the electrical properties of the conductor. This discrete circuit component approach has been previously successfully applied to electrode geometries consisting of a
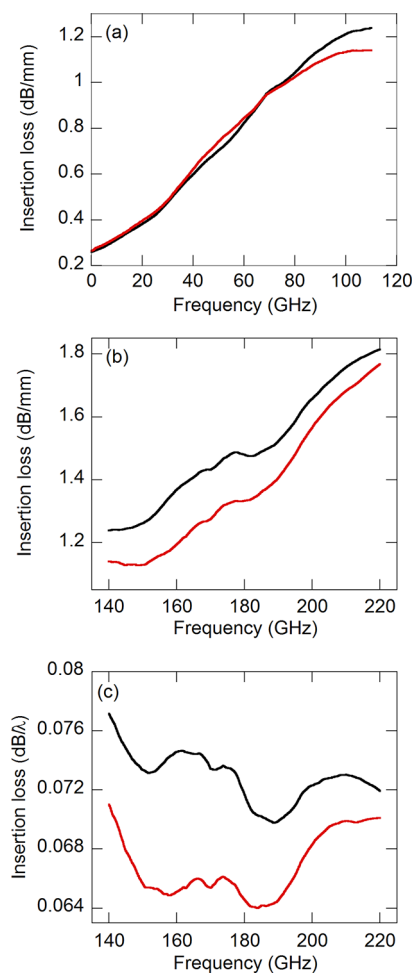
Figure 3. Average electrical loss characteristics from five Ag (black curve) and five *n*Ag (red curve) CPWs in the frequency range (a) 45 MHz to 110 GHz, (b) 140–220 GHz, and c as in b but with the loss expressed as dB per wavelength (dB/λ).

number of nanoconductors such as single carbon nanotubes (CNTs) or small bundles of nanotubes.[21] However, this approach is only valid when the electrical length of the conductor is no more than about 1/20 of the signal wavelength.[20] For example, in the study of the electrical characteristics of CNTs by Jun et al.,[21] the CNT was 7 μm long and at 50 GHz, we calculate that the electrical length in that study to be 0.0027λ, safely below the 0.05λ limit. For our 25 mm long conductors, we calculate the electrical length at 10 GHz to be 1.9λ, which is clearly much longer than 0.05λ. However, despite this limitation, we can still explain the electrical results obtained.

In a recent study by some of us, the high frequency characterization of carbon nanotube (CNT)–polymer nanocomposites based conductors with 10 wt % CNT content, also revealed low electrically losses.[19] In that study, it was proposed that the enhanced electrical conduction was brought about because of capacitive coupling between individual or small bundles of nanotubes. The overall impedance was found to be controlled by the impedance associated with the capacitive behavior which decreased at higher frequencies and was the reason for the improved conduction. The evidence for the importance of capacitive coupling came from the presence of large phase shifts made on the CNT nanocomposite CPWs. It is well-known[22] that when an electromagnetic wave propagates

through a medium the propagation constant, γ, is a complex quantity with the real component, α, associated with attenuation and an imaginary term, β, associated with the phase change per unit length, that is, $\gamma = \alpha + j\beta$. The overall phase may change as a function of the length of the line (Δl) and for most materials can be expressed as $\Delta\phi = \beta\Delta l$. We have made phase shift measurements on the nAg and Ag CPWs, of the same length, 5 and 25 mm, in both frequency bands, and found no consistent trend in the phase data. The absence of a consistent phase shift strongly suggests that we can neglect the effects of any significant capacitive coupling (and inductive effects) between the silver grains or between the nanoparticles with any residual polymer coating as a primary reason for the improved characteristics. The nAg samples can then be considered as nearly an entirely conductive phase with only a small (if any) amount of PMMA present acting a very thin layer. By contrast, the samples of ref 19 consist of 10 wt % carbon nanotubes with the remainder being PMMA polymer. As a consequence the two sets of samples thus represent different ends of the conductor−insulator−conductor family of systems with a high content of conductor in the present system and a lower content in the nanotube system.

To explain the lower electrical losses found in the nAg CPWs, it is worth recalling that the electrical loss of a conductor has both a bulk and surface component; the importance of the latter becoming more and more important at higher frequencies as the skin depth of the conductor is reducing. The similarity of the losses in the lower frequency range (Figure 3a) suggests that the overall electrical loss is being determined by the bulk properties of the two conductors; however, at the higher frequency range (Figure 3b) the contribution played by currents near the surface plays an ever increasingly important role. From the electron microscope and AFM images of Figure 2, it is clear that the packing of Ag nanoparticles is better than that of thick film Ag sample with the result that the former has a lower surface roughness than the latter by about a factor of 3. This higher packing and lower roughness results in enhanced electrical conduction and lower losses at the higher frequencies.

Control of the surface roughness of the conductor at high frequencies is, therefore, a general important material consideration in device fabrication. These results here demonstrate that metallic nanoparticles offer superior electrical performance than conventional high temperature thick film metals. The added advantage of the use of lower sintering temperatures may also find applications in flexible high frequency electronics, which employ temperature sensitive substrate, such as antennas on curved surfaces. Furthermore the characteristics of SRR microwave metamaterials are known to depend on the ohmic resistance because of damping and the energy lost by radiation loss.[23] Controlling the ohmic losses will therefore result in improved transmission resonance characteristics and the Q factor of SRRs. Our results demonstrate that between 80−220 GHz that nAg based materials have reduced electrical loss over conductors made from micrometer-sized grains of silver.

4. CONCLUSION

In summary, we have characterized the high frequency electrical behavior of nAg based conductors up to 220 GHz. We have shown that for frequencies in excess of 80 GHz the electrical losses from samples fabricated from silver nanoparticles are lower than similar conductors fabricated using thick film silver

conductors fired at much higher temperatures. The lower loss at higher frequency is attributed to the lower surface roughness found with the nanoparticles due to better packing and may open opportunities for low temperature fabrication of antennas and for sub-THz metamaterials with improved performance.

■ AUTHOR INFORMATION

Corresponding Author
*E-mail: David.Carey@surrey.ac.uk.
Notes
The authors declare no competing financial interest.

■ REFERENCES

(1) Lei, Y.; Mehmood, F.; Lee, S.; Greeley, J.; Lee, B.; Seifert, S.; Winans, R. E.; Elam, J. W.; Meyer, R. J.; Redfern, P. C.; Teschner, D.; Schlögl, R.; Pellin, M. J.; Curtiss, L. J.; Vajda, S. *Science* **2010**, *328*, 224−228.
(2) Liu, N.; Tang, M. L.; Hentschel, M.; Giessen, H.; Alivisatos, H. P. *Nat. Mater.* **2011**, *10*, 631−636.
(3) Brongersma, M. L.; Shalaev, V. M. *Science* **2010**, *328*, 440−441.
(4) Atwater, H. A.; Polman, A. *Nat. Mater.* **2010**, *9*, 205−213.
(5) Henley, S. J.; Carey, J. D.; Silva, S. R. P. *Appl. Phys. Lett.* **2006**, *88*, 081904.
(6) Roduner, E. In *Nanoscopic Materials: Size-Dependent Phenomena*, 1st ed.; Royal Society of Chemistry Publishing: London, 2006; p 136.
(7) Magdassi, S.; Grouchko, M.; Berezin, O.; Kamyshny, A. *ACS Nano* **2010**, *4*, 1943−1948.
(8) Attarian Shandiz, M. *J. Phys.: Condens. Matter* **2008**, *20*, 325237.
(9) Yeshchenko, O. A.; Dmitruk, I. M.; Alexeenko, A. A.; Kotko, A. V. *Nanotechnology* **2010**, *21*, 045203.
(10) Little, S. A.; Begou, T.; Collins, R. W.; Marsillac, S. *Appl. Phys. Lett.* **2012**, *100*, 051107.
(11) Gunawan, L.; Johari, G. P. *J. Phys. Chem. C* **2008**, *112*, 20159−20166.
(12) Ko, S. H.; Pan, H.; Grigoropoulos, C. P.; Park, I.; Pisano, A. P.; Luscombe, C. K.; Fréchet, J. M. J. *Nano Lett.* **2007**, *7*, 1869−1877.
(13) Henley, S. J.; Carey, J. D.; Silva, S. R. P. *Appl. Phys. Lett.* **2004**, *84*, 4035−4037.
(14) Allen, M. L.; Aronniemi, M.; Mattila, T.; Alastalo, A.; Ojanperä, K.; Suhonen, M.; Seppä, H. *Nanotechnology* **2008**, *19*, 175201.
(15) Redinger, D.; Molesa, S.; Yin, S.; Farschi, R.; Subramanian, V. *IEEE Trans. Electron Devices* **2004**, *51*, 1978−1983.
(16) Shaker, G.; Safavi-Naeini, S.; Sangary, N.; Tentzeris, M. M. *IEEE Antennas Wireless Propag. Lett* **2011**, *10*, 111−114.
(17) Komoda, N.; Nogi, M.; Suganuma, K.; Kohno, K.; Akiyama, Y.; Otsuka, K. *Nanoscale* **2012**, *4*, 3148.
(18) Walther, M.; Ortner, A.; Meier, H.; Löffelmann, U.; Smith, P. J.; Korvink, J. G. *Appl. Phys. Lett.* **2009**, *95*, 251107.
(19) Alshehri, A. H.; Jakubowska, M.; Sloma, M.; Horaczek, M.; Rudka, D.; Free, C.; Carey, J. D. *Appl. Phys. Lett.* **2011**, *99*, 153109.
(20) Pozar, D. M. In *Microwave Engineering*, 3rd ed.; Wiley-Interscience: New York, 2004; p 56.
(21) Jun, S. C.; Choi, J. H.; Cha, S. N.; Baik, C. W.; Lee, S.; Kim, H. J.; Hone, J.; Kim, J. M. *Nanotechnology* **2007**, *18*, 255701.
(22) Griffiths, D. J. In *Introduction to Electrodynamics*, 3rd ed.; Prentice Hall: Upper Saddle River, NJ, 1999; p 364.
(23) Singh, R.; Azad, A. K.; O'Hara, J. F.; Taylor, A. J.; Zhang, W. *Opt. Lett.* **2008**, *33*, 1506−1508.